

System Design, Modelling, and Tracking Filter for Bearings Only Analog Camera

Joel Shields, Richard Bailey, Brent Lytle, Jeff Schroeder, Boris Lurie, Ahmet Behcet Acikmese, Guru Singh, Jason Keim, Asif Ahmed

Abstract—The Formation Control Testbed (FCT) is a ground based multiple robot testbed for simulating the dynamic interaction of spacecraft formations in a representative 6-DOF environment. Linear and spherical air bearings are used to mimic the drag free space environment. Each robot is fully autonomous with a self contained supply of float gas, integrated battery power, and a complete suite of onboard avionics including IMU (3-axis gyro), wireless interspacecraft and ground communication links, cold-gas thrusters, and reaction wheels.

For attitude determination each robot uses an analog camera to image IR beacons fixed to the walls and ceiling of the test facility. These navigation beacons act as an artificial star field. Due to the close proximity of these beacons, the camera direction measurements are coupled to both translation and attitude maneuvers of the robot. This allows unique determination of each quantity, provided enough beacons are in the camera FOV. We have come to refer to this sensing scheme as the “Celestial Sensor”.

In this paper, each subsystem of the Celestial Sensor is discussed with emphasis given to the filtering algorithms. The celestial sensor software processes sequential frame based bearing measurements on a peripheral CPU specifically designed for this application. A frame preprocessor is used to normalize each bearing measurement and apply a number of accept/reject rules. The accepted set of measurements is then passed to an Extended Kalman Filter (EKF) that is tuned to track the motion of the robot within the room.

A detailed sensor model is described that is used to predict the performance of the integrated system. Frame based simulations using this sensor model are presented that predict 1-sigma errors on the order of 3.0 arc minutes in attitude (per axis) and 4.0 millimeters in position (per cartesian coordinate). Preliminary results from the production system are given that demonstrate uncalibrated functional operation of the system.

I. INTRODUCTION

The problem of indoor navigation has been motivated by a number of diverse applications including virtual reality, photogrammetry, aircraft assembly, and robotic operations. Researchers have characterized these applications in two categories, “outside-looking-in” applications, such as photogrammetry, where the sensing is done external to the vehicle or target of interest and “inside-looking-out” applications where the sensing of external landmarks is done on-board. Examples of the latter are the Arc Second

J. Shields, J. Schroeder, B. Lurie, A. Acikmese, G. Singh, J. Keim, and A. Ahmed are with the Jet Propulsion Laboratory, California Institute of Technology, 4800 Oak Grove Drive, Pasadena, CA 91109-8099, Joel.F.Shields@jpl.nasa.gov

R. Bailey and B. Lytle are with Automated Controlled Environments Inc., 25133 Ave Tibbitts Unit A, Valencia, CA 91355, rbailey@acei-ca.com

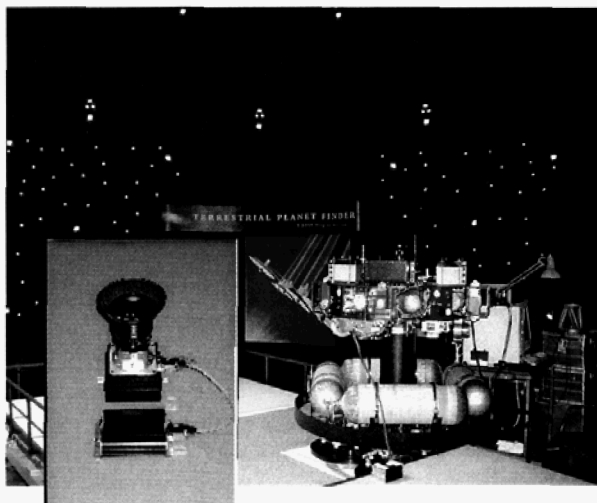


Fig. 1. Photograph of the FCT robot in the Formation Flying Technology Laboratory at JPL. The top attitude stage is supported by a spherical air bearing. Linear air bearings support the entire robot on a precision ground flat floor. Inset shows celestial sensor optics and preamps which are mounted in the center of the attitude stage.

Constellation^{3Di} Indoor-GPSTM system [1], [2] and the UNC HiBall Tracker [3], [4]. The FCT robots require the “inside-looking-out” architecture as they must have on-board knowledge of their positions and attitudes.

Our system uses high power (1200 mW at 800 mAmps) modulated IR (940nm) beacons as navigation reference points. Each of these beacons contains a 6mm square array of 60 high efficiency LEDs. Directions to these reference points are sensed with a large format, wide field of view camera (Canon FD 24mm f1.4, 84 deg. FOV). The camera is configured with a 45mm x 45mm silicon position sensing detector (PSD). This detector is a solid state four terminal device used to sense the spot position in two directions. The photocurrents from the bottom two terminals, or anodes, are used to determine the spot position in one direction, and the top two terminals, or cathodes, are used to determine the spot position in a perpendicular direction. Because these detector currents change with both spot position and light intensity, the signals are normalized in software to eliminate the intensity dependence.

Since the detector senses only the center of light, the beacons are imaged one by one in a sequential manner

each beacon. Each frame starts with a 0.75 millisecond sync pulse that is used by the electronics on the sensor side to trigger sampling of the detector waveforms. After the sync pulse, the electronics turn off all the beacons for 3.0 milliseconds to allow for calibration of the ambient light conditions. The beacons are then turned on one at a time in a specific sequence that the sensor software has prior knowledge of. This allows temporal association of a particular waveform sample to a given beacon which is essential for processing of the bearing measurements. The remainder of the frame is left vacant to allow for expansion from the current 34 beacon design.

The beacon electronics perform closed loop current control each time a beacon is turned on. The rise time is approximately 20.0 microseconds, accounting for only a small portion of the total on time. The amount of current assigned to each beacon during the sync and strobe operations is fixed from frame to frame but is a programmable quantity. Beacons that are generally imaged from long distances can have more current assigned to them to increase the signal strength at the detector. Beacons imaged at close distance, such as those on the walls need to be dimmer so as to not saturate the detector. Typically beacon currents range from 1.3 amps to 300.0 milliamps depending on location. In addition to current, the time slots, sync subset and frame rate are all programmable quantities.

B. Sensor Head Optics and Electronics

The sensor head uses a newly available large format silicon detector (On Trak PSM2-45). This detector allows the use of standard 35mm format lenses with large collecting apertures. The detector is sensitive to wavelengths between 600 nm and 1200 nm with a peak sensitivity at 940 nm. A long pass cutoff filter (RG850) is used just in front of the detector and behind the lens to reduce the sensitivity of the detector to visible and other sources below wavelengths of 800 nm.

1) *Analog Electronics:* The four detector photocurrents are amplified by a simple two stage preamp based on Analog Devices AD8605 op amp. This first stage is an inverting transimpedance amplifier with a gain of $1e6$ that is AC coupled to the signal currents. The AC coupling is necessary because it eliminates the variation of the amplifier output to slowly changing thermal transients. Without AC coupling we have noticed the output swings by as much as 2.0 volts of the 5.0 volt range over a 24 hour cycle. This corresponds to a thermal current variation of ± 100.0 nAmps.

The second stage of the amplifier is a summer stage that amplifies the signal path by a factor of -7 and adds a constant offset to the signal. The offset is introduced to take maximum advantage of the available input range of the A2D converters by allowing for the largest possible signal level variations. When light falls on the detector, signal current flows from the X terminals (anodes) through the device to the Y terminals (cathodes). Thus, the X and Y signals have

opposite signs and should be placed near opposite rails of the 5 volt input range. The offset stage of the amplifier is used to put the X signals near the top 5.0 volt rail and the Y signals near the bottom 0.0 volt rail. In this way the negative X currents get inverted twice and swing negative toward zero volts. The positive Y current get inverted twice and swing positive toward 5.0 volts.

2) *Digital Electronics:* The processor used to implement the tracking filters is a TI TMS320C6713 floating point DSP capable of 1.0 GFLOP. A Xilinx FPGA runs a sync detection algorithm and buffers 80.0 microsecond sampled frame data before passing it to the DSP. Four 16 bit A2D converters are used to sample the preamp outputs. The DSP board has two serial output ports used to pass processed frame data to either the main robot CPU or a diagnostic port.

III. SENSOR MODEL

The total current, I_{signal} , generated by the detector in response to a beacon is modelled using the following equation.

$$I_{signal} = D_R \cdot G_{glass} \cdot G_L(\theta_L) \cdot G_B(\theta_B) \cdot \frac{\pi R_A^2}{D^2} \cdot (P_1 \cdot I_B), \quad (1)$$

where I_B is the beacon current, $P_1 = 0.4375$ (W/sr/amp) is the radiant intensity coefficient of the beacon in units of watts per steradian per amp, $R_A = 0.0086$ (m) is the aperture radius, and D is the distance between a given beacon and the focus of the camera which depends on the robot position and attitude. $G_B(\theta_B)$ is the off-axis attenuation of the beacon brightness which was experimentally determined to be $G_B(\theta_B) = \cos(0.85 \theta_B)$. $G_L(\theta_L)$ is the off-axis attenuation of the lens which was experimentally determined to fit a cosine power law of the form, $G_L(\theta_L) = \cos^{2.5}(\theta_L)$. G_{glass} is the attenuation of the optics and was experimentally determined to be 0.33 based on direct measurements of the detector currents and known beacon radiant intensity. $D_R = 0.63$ (amps/watt) is the detector responsivity at wavelengths of 940 nm.

Equation (1) gives the sum of the current at each anode of the detector which is proportionately assigned to each terminal based on the spots focal plane position. For example, the currents assigned to each of the Y terminals is given by,

$$i_{Y1} = \frac{I_{signal}}{D_L} y_{fp} + \frac{I_{signal}}{2} \quad (2)$$

$$i_{Y2} = I_{signal} - i_{Y1}, \quad (3)$$

where $D_L = 0.045$ (m) is the size of the detector and y_{fp} is the position of the spot from the center of the array in the y-direction. Similar equations apply for the X currents except that they have opposite sign. The spot position, (x_{fp}, y_{fp}) , is determined using a model of the lens optical properties.

For this purpose we use a simple pinhole type model,

$$V_{Nx} = k_g \arctan (G_a \cdot (\hat{v}_{FOCUS \rightarrow B_i}^S(x) / \hat{v}_{FOCUS \rightarrow B_i}^S(z))) \quad (4)$$

$$V_{Ny} = k_g \arctan (G_a \cdot (\hat{v}_{FOCUS \rightarrow B_i}^S(y) / \hat{v}_{FOCUS \rightarrow B_i}^S(z))), \quad (5)$$

where $\hat{v}_{FOCUS \rightarrow B_i}^S$ is the unit vector from the focus of the lens to a given beacon, cast in the frame of the sensor, S . The left hand side of these equations are the normalized focal plane measurements $V_{Nx}, V_{Ny} \in [-1, 1]$, and are linear functions of the spot position, e.g. $V_{Nx} = 1$ when $x_{fp} = D_L/2$ and $V_{Nx} = -1$ when $x_{fp} = -D_L/2$. Determining these variables from the preamp voltages is covered in section IV. The sensor model uses Equations (4)-(5) to compute what these quantities would be for a given beacon direction. Equations (2)-(3) and their equivalents for the X currents are then used to determine the four detector signal currents $i_{X1}, i_{X2}, i_{Y1}, i_{Y2}$. k_g and G_a are curve fit parameters that were experimentally determined by rotating the camera about its focus using precise knowledge of the beacon location and sensor frame orientation. We are currently using a 6 axis hexapod (PI M850) for accurate calibration of the focal plane. For the 24mm Canon lens k_g was determined to be $1.5 (1/rad.)$ and $G_a = 0.75$.

The unit vector given in Equations (4)-(5) depends on both the robot position and attitude. To represent the attitude of the robot avionics platform we use roll, pitch, and yaw Euler angles,

$${}^B \mathbf{R}^{JC}(\gamma, \beta, \alpha) = \mathbf{R}_Z(\gamma) \mathbf{R}_Y(\beta) \mathbf{R}_X(\alpha). \quad (6)$$

The matrix ${}^B \mathbf{R}^{JC}$ is to be interpreted passively, meaning it will express room frame, JC , vectors in the body frame, B , of the robot's attitude stage. To reference the location of the robot we use the center of rotation of the spherical air bearing,

$$\mathbf{v}_{CR}^{JC} = [x_{CR}, y_{CR}, z_{CR}]^T. \quad (7)$$

The vector to a given beacon, B_i , in the array can then be written as,

$$\mathbf{v}_{FOCUS \rightarrow B_i}^S = {}^S \mathbf{R}^B [({}^B \mathbf{R}^{JC}(\gamma, \beta, \alpha))^T (\mathbf{v}_{B_i}^{JC} - \mathbf{v}_{CR}^{JC}(x_{CR}, y_{CR}, z_{CR})) - \mathbf{v}_{CR \rightarrow FOCUS}^B], \quad (8)$$

with its direction given by,

$$\hat{\mathbf{v}}_{FOCUS \rightarrow B_i}^S = \frac{\mathbf{v}_{FOCUS \rightarrow B_i}^S}{\|\mathbf{v}_{FOCUS \rightarrow B_i}^S\|}. \quad (9)$$

The robot state variables, $\mathbf{x} = [\alpha, \beta, \gamma, x_{CR}, y_{CR}, z_{CR}]^T$, are generated from a thruster based dynamic model of the robot motion. Various maneuvers can be programmed by adjusting the 16 thruster on times. The beacon currents seen in Equation (1) are generated from a simulation of the beacon switching electronics. Transfer function models of the beacon current control loops and analog electronics were used to determine the four preamp voltages from the detector signal currents. This model included additive white

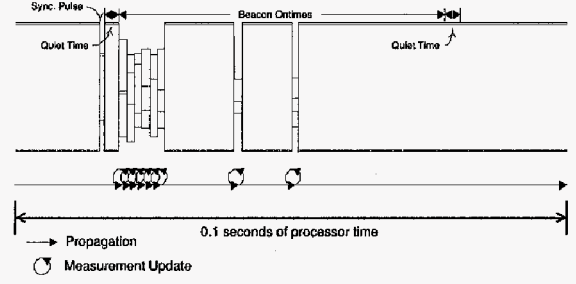


Fig. 4. Estimation time line. Measurements are processed sequentially using internally generated frame relative time tags.

noise to each output channel. Measurements taken from the actual preamp indicated 1-sigma Gaussian noise on the order of 1.3 mV.

IV. ALGORITHMS

A. Frame Preprocessor

The frame data passed to the estimator code is an 80.0 microsecond, 16 bit sampled time series of the 4 detector signals starting immediately after the detection of the sync pulse. The first 3.0 milliseconds of the frame is dark time used to calibrate bias voltages. This is followed by the 34, 1.5 millisecond, beacon on times and concludes with an additional 3.0 millisecond calibration interval. Figure 5 in section V shows a typical frame.

Before the estimator code can be executed, the raw sampled frame data must be cast in terms of measurements that have physical meaning. The opportunity is also taken to exclude data that doesn't pass a number of quality checks. If the signal levels for a given beacon do not exceed a threshold value specified in the software they are determined to be outside the FOV or inside the FOV but too dim (far away) to be of much use. We also eliminate beacons determined to be near the FOV edge. This is because they are likely to have poor repeatability due to optical distortions. Each beacon is sampled approximately 18 times during a given exposure. The ten samples nearest the center of the on time are used to determine the voltage level. Both the mean and standard deviation of these samples are calculated. If the standard deviation is larger than would be expected based on the known preamp noise, we discard this measurement as well. This protects the filter from transient electrical perturbations and from using a beacon that traversed through the FOV edge during an exposure.

For each beacon that passes the editing process, we calculate the following normalized measurements of the focal plane spot position,

$$V_{Nx} = \frac{(V_{X1} - V_{X1_{bias}}) - (V_{X2} - V_{X2_{bias}})}{(V_{X1} - V_{X1_{bias}}) + (V_{X2} - V_{X2_{bias}})} \quad (10)$$

$$V_{Ny} = \frac{(V_{Y1} - V_{Y1_{bias}}) - (V_{Y2} - V_{Y2_{bias}})}{(V_{Y1} - V_{Y1_{bias}}) + (V_{Y2} - V_{Y2_{bias}})} \quad (11)$$

$V_{Nx}, V_{Ny} \in [-1, 1],$

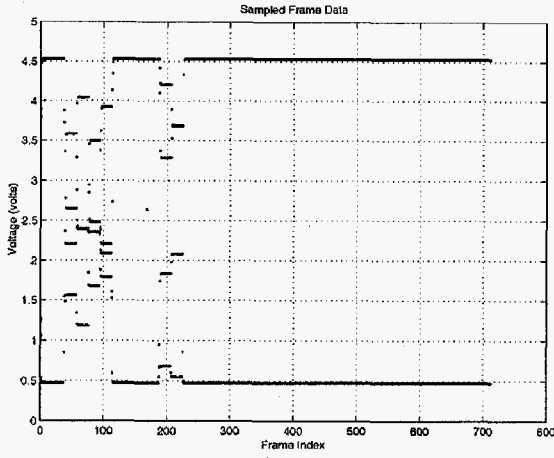


Fig. 5. Simulated frame data. Beacons 1 through 4 and 9 through 10 are within the camera FOV.

where V_{X1} , V_{X2} , V_{Y1} and V_{Y2} are the mean voltage levels during the on time. The bias voltages for each beacon, $V_{X1_{bias}}$, $V_{X2_{bias}}$, $V_{Y1_{bias}}$, and $V_{Y2_{bias}}$ in Equations (10)-(11) are based on a linear interpolation of the mean bias voltages calculated before and after strobing. Each of these means is based on 20 samples during the dark calibration intervals.

B. EKF

Let us define the state vector for the estimation problem to be,

$$\mathbf{x} = [\alpha, \beta, \gamma, x_{CR}, y_{CR}, z_{CR}]^T. \quad (12)$$

Our measurements can then be written as a function of this state in the standard nonlinear form;

$$\mathbf{y} = \mathbf{h}(\mathbf{x}) + \mathbf{v}(t). \quad (13)$$

The left hand side of this equation are the bearing measurements calculated using Equations (10)-(11). The first term on the right hand side, $\mathbf{h}(\mathbf{x})$, is the model of the nonlinearity given by substituting Equations (6)-(9) into Equations (4)-(5). To calculate $\mathbf{h}(\mathbf{x})$, the transformation between the sensor and body frames, ${}^S\mathbf{R}^B$, and focus location, $\mathbf{v}_{CR \rightarrow FOCUS}^B$, are assumed known. We are presently determining these quantities off line. The second term on the right hand side of Equation (13) is the noise associated with the measurement variables V_{Nx} and V_{Ny} . If we let,

$$\mathbf{J}_{V_{Nx}} := \frac{\partial V_{Nx}}{\partial [V_{X1}, V_{X1_{bias}}, V_{X2}, V_{X2_{bias}}]}, \quad (14)$$

then $\sigma_{V_{Nx}}^2$ is related to the preamp noise, $\sigma_v = 1.3 \text{ mV}$, by,

$$\sigma_{V_{Nx}}^2 = \mathbf{J}_{V_{Nx}} \begin{bmatrix} \frac{1}{10}\sigma_v^2 & 0 & 0 & 0 \\ 0 & \frac{1}{20}\sigma_v^2 & 0 & 0 \\ 0 & 0 & \frac{1}{10}\sigma_v^2 & 0 \\ 0 & 0 & 0 & \frac{1}{20}\sigma_v^2 \end{bmatrix} \mathbf{J}_{V_{Nx}}^T, \quad (15)$$

where we have assumed that the four signals V_{X1} , $V_{X1_{bias}}$, V_{X2} , and $V_{X2_{bias}}$ are uncorrelated with other. This is a good

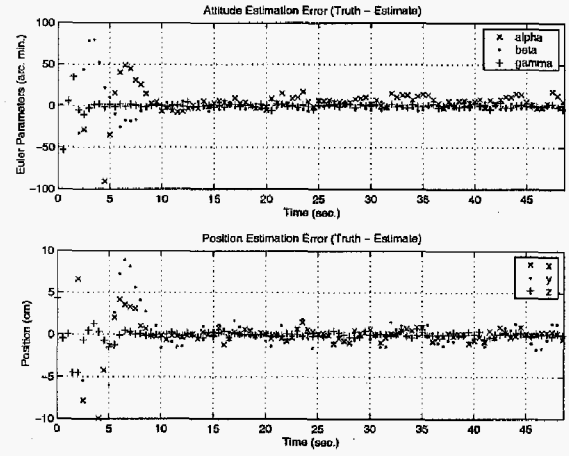


Fig. 6. Simulated state estimation errors. Euler parameters shown in top subplot. Position errors shown in bottom plot. Thruster event at $t = 20.0$ seconds causes negative rotation about the y -axis.

assumption if each of the preamp voltages are uncorrelated with each other and each has a small correlation time relative to the exposure time. The mean values of V_{X1} , $V_{X1_{bias}}$, V_{X2} , and $V_{X2_{bias}}$ calculated in the preprocessor are used to evaluate $\mathbf{J}_{V_{Nx}}$. Note that the term,

$$V_{\Sigma} = [(V_{X1} - V_{X1_{bias}}) + (V_{X2} - V_{X2_{bias}})]^2, \quad (16)$$

appears in the denominator of the elements in $\mathbf{J}_{V_{Nx}}$. V_{Σ} is an indicator of signal strength. Measurements with large V_{Σ} will have less uncertainty. Equation (15) and its equivalent for $\sigma_{V_{Ny}}^2$ are used in the estimator code for optimal filter tuning.

Note that \mathbf{y} in Equation (13) is a 2×1 vector of a single bearing measurement. At least three such measurements within the time constant of the filter are required to uniquely solve for the state \mathbf{x} and maintain stability of the filter. Since the measurements arrive sequentially at different times with a given frame, we choose to process them in the same manner, one at a time, until the entire onset has been processed (See Figure 4).

The EKF requires that the Jacobian of $\mathbf{h}(\mathbf{x})$ be computed at each iteration of the filter using the propagated value of the state estimate, $\hat{\mathbf{x}}(k-)$ [6]. To estimate this derivative a central difference technique with fixed step size was used.

To model how the state changes with time we use a random jerk process model, e.g.,

$$\ddot{\mathbf{x}} = \mathbf{w}. \quad (17)$$

where \mathbf{w} is used as a tuning parameter of the filter. This model theoretically allows the estimator to track ramp trajectories of the robot position and attitude with zero error. Although this model does not require knowledge of the input function, in this case the thruster activity, to propagate the estimator states this simplicity comes at a price. In order to track through thruster events without transient errors, the measurements have to be given strong weight by making \mathbf{w}

larger in proportion to v . This in turn reduces the smoothing and reduction in variance that would otherwise be achieved with this model. With these constraints in mind, we tune the filter to give as much smoothing of the estimates as possible without sacrificing too much in the way of transient errors during thruster activity. Simulations are given in section V that illustrate the performance achieved under the constraints of this tradeoff.

V. SIMULATIONS

In this section we present simulation results of the system to characterize the achievable performance. The simulations use a 2 Hz instead of a 10 Hz update rate to match the update rate of the currently deployed system. The sensor model described in section III was used to generate raw 10 Hz frame data. Every fifth frame was extracted from this data set and uploaded to the celestial sensor software one frame at a time. This editing process preserved the actual frame set seen by the deployed system. Figure 5 shows a typical frame near the end of the simulated maneuver.

The robot was initially placed at,

$$\mathbf{x}(t_0) = [0.01745 \text{ (rad.)}, 0.0349 \text{ (rad.)}, 0.05236 \text{ (rad.)}, \\ 0.1 \text{ (m)}, 1.5 \text{ (m)}, 1.33 \text{ (m)}]^T. \quad (18)$$

At $t = 20.0$ seconds, thrusters were fired that rotated the attitude stage by -0.1458 (deg./sec.) about the x -axis of the body frame.

Figure 6 shows a plot of the position estimation errors. The initial transient at the start is due to the large mismatch between the initial estimate of the robot state and the actual location. In the absence of any information the code assumes the robot is in the center of the room with the body frame aligned to the room frame. After the transient dies down, the residual rms errors are on the order of 3.0 arc minutes in attitude and 0.4 centimeters in position, with no noticeable increase in errors during the thruster event.

VI. EXPERIMENTAL RESULTS

The first open loop tests of the sensor are reported in this section. Since no independent means of checking the sensor output is available without a redundant sensing scheme, only functional results can be reported at this time. The experiment we performed started with the attitude stage air bearing unpressurized and the lens cap of the sensor in place. With the lens cap on, the celestial sensor digital electronics was unable to see the sync pulse and as a result no frame data was captured. In the absence of DSP data, the robot telemetry software sends zeros to the ground station. This is what we see at the beginning of Figure 7. At $t \approx 2800$ seconds the lens cap was removed, sync was detected, and the estimates converged to the values shown. Three minutes later we pressurized the air bearing and floated the attitude stage, stabilizing it manually. Holding the attitude stage by hand we first rotated the air bearing about the positive x -axis by about 5.0 degrees, then about the y -axis by roughly the same amount as we could determine visually.

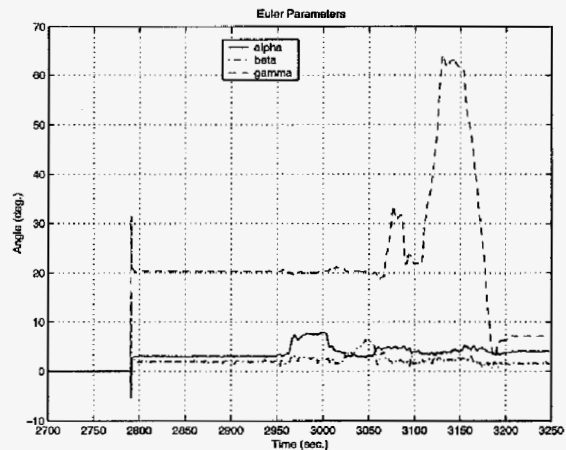


Fig. 7. Robot telemetry stream coming from wireless RF modem. Estimated celestial sensor attitude parameters are shown.

We then returned to level and did two large rotations about the spin axis, the second bigger than the first. The telemetry data in Figure 7 corresponds to what you would expect to see based on the testing sequence.

VII. CONCLUSIONS AND FUTURE WORKS

In this paper we have presented the first milestone results in the development of the FCT navigation system. Future efforts will include the development of an estimator for mixing of the gyro data (KVH DSP 3000) and celestial sensor attitude estimates. This filter will be designed to smooth the celestial sensor attitude estimates to the sub. arc minute level and correct the gyro measurements for bias variations. The celestial sensor estimator will undergo further refinement including a more comprehensive calibration of the focal plane and accurate measurement of the sensor offset and orientation. The focal plane model used in this paper was based on a simple two axis calibration and assumes off axis areas of the focal plane have no deviation from this model.

The celestial sensor software also needs an initialization routine to avoid the long convergence times of the tracking filter detailed in this paper. This will also ensure global convergence of the solution regardless of the initial robot pose, provided enough beacons are in the FOV [7]. We have found that the tracking filter can diverge if the initial position errors are on the order of several meters and or attitude errors are on the order of 40 degrees.

We are also exploring using a photogrammetry system (Geodetic INCA2) to survey the LED positions directly. This technique is able to determine the beacon locations remotely using a bundle of digital photographs.

VIII. ACKNOWLEDGMENTS

The authors gratefully acknowledge the funding of NASA and the Terrestrial Planet Finder Project. The work described in this paper was carried out at the Jet Propulsion

Laboratory, California Institute of Technology, under contract with the National Aeronautics and Space Administration.

REFERENCES

- [1] "Error Budget and Specifications", *Arc Second White Paper 063102*, Dulles, VA, 2002.
- [2] "Indoor GPS Technology For Metrology", *Arc Second White Paper 071502*, Dulles, VA, 2002.
- [3] G. Welch and G. Bishop and L. Vicci and S. Brumback and K. Keller and D. Colucci, "The HiBall Tracker: High-Performance Wide-Area Tracking for Virtual and Augmented Environments", *Proceedings of the ACM Symposium on Virtual Reality Software and Technology*, University College, London, December, 1999.
- [4] G. Welch and G. Bishop and L. Vicci and S. Brumback and K. Keller, High-Performance Wide-Area Optical Tracking, The HiBall Tracking System, *Presence: Teleoperators and Virtual Environments*, vol. 10, no. 1, February, 2001.
- [5] D. Qian and W. Wang and I. J. Busch-Vishniac and A. B. Buckman, A Method for Measurement of Multiple Light Spot Positions on One Position Sensitive Detector (PSD), *IEEE Transactions on Instrumentation and Measurement*, vol. 42, no. 1, February, 1993, pp 14-18.
- [6] A. Gelb, *Applied Optimal Estimation*, The M.I.T. Press, Cambridge, MA; 1974.
- [7] A. Ansar and K. Daniilidis, Linear Pose Estimation from Points or Lines, *IEEE Transactions on Pattern Analysis and Machine Intelligence*, vol. 25, no. 5, May, 2003, pp 578-589.
- [8] C. Lu and G. Hager and E. Mjolsness, Fast and Globally Convergent Pose Estimation from Video Images, *IEEE Transactions on Pattern Analysis and Machine Intelligence*, vol. 22, no. 6, June, 2000, pp 610-621.
- [9] C. Poelman and T. Kanade, A Paraperspective Factorization Method for Shape and Motion Recovery, *IEEE Transactions on Pattern Analysis and Machine Intelligence*, vol. 19, no. 3, March, 1997, pp 206-218.